Work Function and Energy Level Alignment Tuning at Ti_3C_2-T_x MXene Surfaces and Interfaces Using (Metal-)Organic Donor/Acceptor Molecules

Thorsten Schultz[1], Peer Bärmann[1], Elena Longhi[2], Rahul Meena[3], Yves Geerts[3,4], Yury Gogotsi[5,6], Stephen Barlow[2,7], Seth R. Marder[2,7,8], Tristan Petit[1], Norbert Koch[1,9]

[1]Helmholtz-Zentrum Berlin für Materialien und Energie GmbH, Berlin, Germany

[2]School of Chemistry and Biochemistry, Georgia Institute of Technology, Atlanta, Georgia, United States

[3]Laboratoire de Chimie des Polymères, Faculté des Sciences, Université Libre de Bruxelles (ULB), Bruxelles, Belgium

[4]International Solvay Institutes for Physics and Chemistry, Brussels, Belgium

[5]A.J. Drexel Nanomaterials Institute, Drexel University, Philadelphia, Pennsylvania, United States

[6]Department of Materials Science and Engineering, Drexel University, Philadelphia, Pennsylvania, United States

[7]Renewable and Sustainable Energy Institute, University of Colorado Boulder, Boulder, Colorado, United States

[8]Department of Chemical and Biological Engineering and Department of Chemistry, University of Colorado Boulder, Boulder, Colorado, United States

[9]Institut für Physik & IRIS Adlershof, Humboldt-Universität zu Berlin, Berlin, Germany

Keywords: photoelectron spectroscopy, push-back effect, heterojunctions, interlayer method, surface terminations

Abstract

Two-dimensional MXenes, with Ti_3C_2-T_x being the most prominent member, show properties that make them promising for a manifold of applications, including electrodes in light emitting diodes, solar cells, and field effect transistors based on organic semiconductors. In these cases, the work function of MXenes plays an important role for the energy level alignment to the subsequently deposited organic layer, as it determines the electron and hole injection barriers. Therefore, methods for controlling the Ti_3C_2-T_x work function should be developed. We demonstrate that, by using thin layers of (metal-)organic donor/acceptor molecules, the work function of Ti_3C_2-T_x can be tuned over a range of more than 3 eV. This enables tuning the energy level alignment to a subsequently deposited organic semiconductor, all the way from intrinsic Fermi level pinning at the highest occupied molecular energy level (minimal hole injection barrier) to pinning at the lowest unoccupied level (minimal electron injection barrier). Furthermore, it is shown that a predominantly

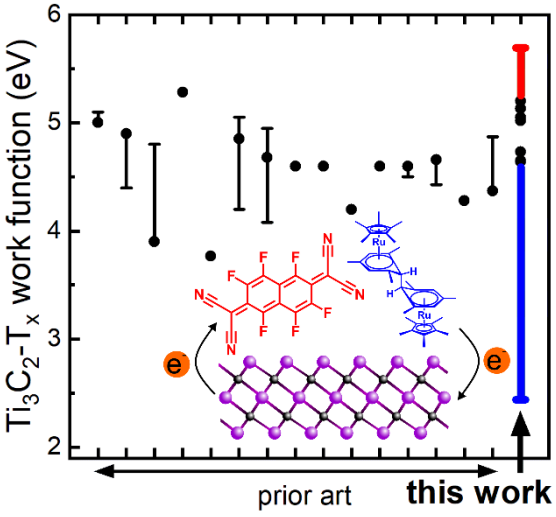

oxygen-terminated surface does not lead to an extraordinary high work function, in contrast to theoretical predictions. The proposed strategy may greatly expand the use of MXenes in conjunction with organic hole and electron transport layers in optoelectronic devices.

Introduction

Since their discovery in 2011 MXenes, which are defined as a family of two-dimensional materials with the formula $M_{n+1}X_n$, where M is a transition metal and X is typically either carbon or nitrogen (oxygen substitution is also possible),[1] have attracted much interest in various fields, including electrochemical energy storage, electromagnetic interference shielding, catalysis, water purification, gas separation, and biomedicine.[2–7] The possibility of employing MXenes to these vastly different fields of application is based on their unique chemical and physical properties, such as high electrical conductivity, processability from aqueous dispersions due to their hydrophilicity, excellent mechanical properties, and, especially, chemical configurability.[8–11]

Recently, MXenes have been employed as electrodes in organic field effect transistors and organic light emitting diodes.[12,13] The high transparency,[14] good electrical conductivity,[15] flexibility,[16] and dispersibility in both water[17] and organic solvents[18] of Ti_3C_2-T_x, although with limited stability, renders it a potential candidate for an electrode material in large scale, flexible devices. The theoretically predicted large tunability of its work function (1.8 eV for pure -OH termination, 6.2 eV for pure -O termination)[19] is another interesting property for this type of application. In combination with the ionization energy (electron affinity) of the semiconductor, the work function directly determines the hole (electron) injection barriers from the electrode to the semiconductor according to the simple Schottky-Mott rule.[20,21] However, the fabrication of MXenes with well-controlled uniform termination remains challenging and no work function values near those predicted have been achieved so far. To the best of our knowledge, the maximum range of intentional work function tuning of Ti_3C_2-T_x experimentally achieved so far is 0.9 eV.[22] A MXene electrode with a perfluorosulfonic acid (PFSA) barrier layer achieved a work function of 5.84 eV and showed promise for organic light-emitting diodes (OLEDs).[23]

In this work, we present an alternative approach to tune the work function of Ti_3C_2-T_x MXene. By using a thin layer of a (metal-)organic electron donor or acceptor molecule (shown in Figure 1, alongside the organic semiconductors employed in this study) the work function of Ti_3C_2-T_x can be adjusted over a remarkably wide range of 3.25 eV. Using these donor/acceptor molecules as an interlayer allowed then to adjust the energy level alignment to a subsequently deposited organic semiconductor from intrinsic Fermi level pinning at the highest occupied molecular orbital (HOMO) level (minimal hole injection barrier) all the way to pinning at the lowest unoccupied molecular orbital (LUMO) level (minimal electron injection barrier). This approach thus enables the optimization of charge injection barriers between Ti_3C_2-T_x and a manifold of organic semiconductors, covering a wide range of ionization energy and electron affinity values. We further show that the work function of predominantly oxygen-terminated Ti_3C_2-T_x is 4.65 eV, much lower than previously predicted,[24] casting doubt on the realizability of extremely high/low predicted work function values by surface termination groups alone.

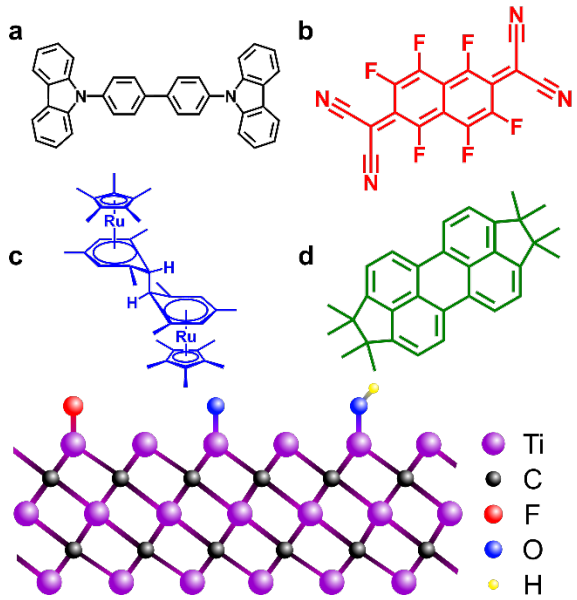

Figure 1: Structure of Ti_3C_2-T_x and of the molecules deposited on top in this work. a) 4,4'-bis(*N*-carbazolyl)-1,1'-biphenyl (CBP), b) 1,3,4,5,7,8-hexafluoro-11,11,12,12-tetracyanonaphtho-2,6-quinodimethane (F_6TCNNQ), c) (pentamethylcyclopentadienyl)(1,3,5-trimethylbenzene)ruthenium dimer ([RuCp*Mes]$_2$) and d) 1,1,2,2,7,7,8,8-octamethyl-1,2,7,8-tetrahydrodicyclopenta[*cd,lm*]perylene (OMP).

Results and discussion

Interfacial push-back effect

Before turning to the work function tuning of Ti_3C_2-T_x with donor/acceptor molecules, we address a fundamental phenomenon that has been revealed before for elemental metal electrodes only. The so-called "push-back" or "pillow" effect describes the reduction of a metal work function after deposition of a layer of non-reactive molecules. The electron density extends outside a bare metal surface, creating a surface dipole that contributes to the overall work function. Upon molecular deposition, this spilling of electron density outside of the surface is reduced by Pauli repulsion with the molecular electron density, resulting in a decrease of the surface dipole and thus the work function.[25] This reduction in work function can be very large, e.g., 1.28 eV in the case of copper.[26] For both inorganic and organic semiconductor surfaces, on the other hand, this effect is typically not observed due to their much lower electron density compared to metals.[27,28] Ti_3C_2-T_x MXene is metallic,[29,30] therefore, in a first step we investigated whether the push-back effect upon molecule deposition is as pronounced as for elemental metals. For this purpose, we chose 4,4'-bis(*N*-carbazolyl)-1,1'-biphenyl (CBP) as organic molecular semiconductor, as it has a sufficiently high ionization energy and suitably low electron affinity (both compared to the work function of our bare MXene surface) to rule out ground state charge transfer related work function changes.[31] The corresponding ultraviolet photoelectron spectroscopy (UPS) spectra are shown in Figure 2. The initial work function of our Ti_3C_2-T_x, as determined from the onset of the secondary electron cut-off (SECO), was 4.65 eV (black curve). Besides a distinct Fermi-edge,

the valence band shows features stemming from fluorine terminations (peak around 0 eV binding energy) and oxygen terminations (peaks at around 2 and 3 eV binding energy) as described in detail in a previous study.[22] After deposition of nominally 5 Å CBP, the work function is reduced slightly to 4.60 eV and further to 4.52 eV after deposition of nominally 15 Å of CBP. The latter corresponds to a closed monolayer, as the work function does not change significantly upon further deposition of CBP. The prominent double-peak structure of the CBP HOMO is clearly visible for nominal thicknesses of 15 Å and above, and yields an ionization energy of 6.16 eV. Adding a value of 3.4 eV for the band gap one obtains an electron affinity of 2.76 eV,[32] confirming that work function changes due to charge transfer can be ruled out as expected. The total 130 meV reduction in work function between bare surface and 15 Å CBP indicates that the push-back effect is comparably small, but not negligible. For comparison, experimental values of work function reduction by the push-back effect reported for elemental metals are 0.95 eV for Ag(111)[33] and 0.8 eV for polycrystalline gold.[34] The small push-back effect observed here is in line with the atomic structure of Ti_3C_2-T_x MXene, where the Ti_3C_2-T_x core features the metallic properties, but the surface termination groups exhibit a more rigid electron density than a bare metal surface, in analogy to what has been reported for a molecularly covered metal.[33] Consequently, Pauli repulsion upon molecule deposition does not change the surface dipole as much as it does for elemental metals.

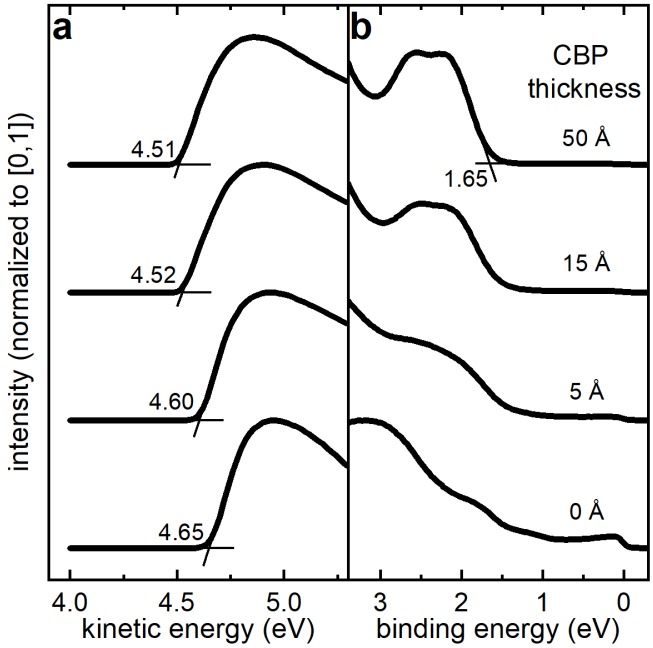

Figure 2: a) Secondary electron cut-off and b) valence band spectra for different thicknesses of CBP deposited on Ti_3C_2-T_x. The reduction in work function can be attributed to the push-back effect. Spectra are vertically offset for clarity.

Work function tuning

Work function modification by using (metal-)organic donor/acceptor molecules has been described before for elemental metals[35,36] and inorganic semiconductors.[28,37–39] The deposition of a thin layer of acceptor molecules with an electron affinity higher than the work function of the substrate leads to an electron transfer from the substrate to the molecular layer to establish electronic equilibrium. This results in the formation of an interface dipole oriented with its positive end toward the substrate, consequently increasing the work function. In the case of inorganic semiconductors a change in surface band bending is typically observed as well, depending on the doping level and surface state density,[40] which further increases the work function. For donor molecules with an ionization energy lower than the substrate work function the concept is reversed. Electrons are transferred from the molecules to the substrate and the resulting interface dipole is oriented with its positive end away from the surface, leading to a decrease in work function. We thus conducted analogous experiments for Ti_3C_2-T_x to investigate whether this strategy can be applied in this case as well.

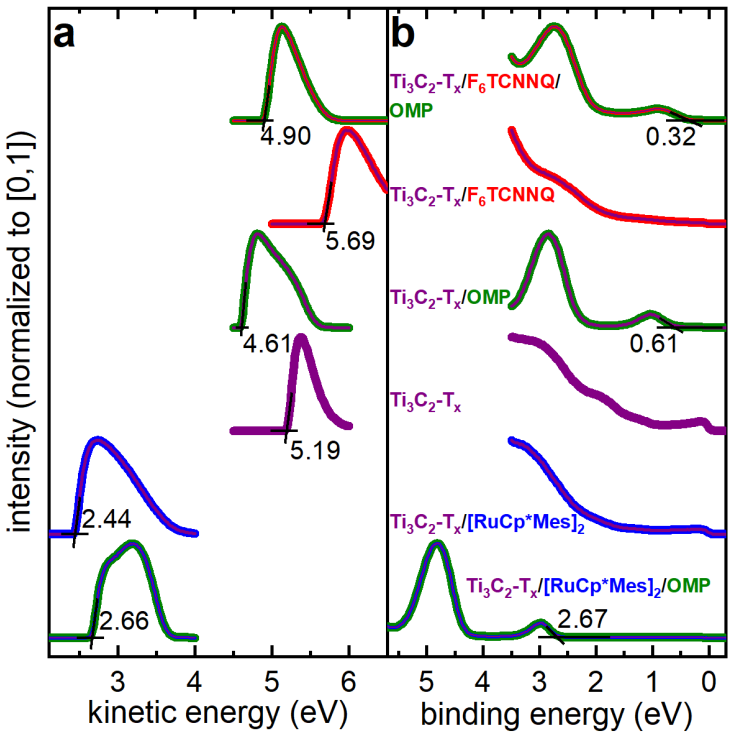

Figure 3: a) Secondary electron cut-off and b) valence band spectra of Ti_3C_2-T_x (black) covered with nominally: 5 nm OMP (green), 1.6 nm F_6TCNNQ (red), 1.6 nm F_6TCNNQ + 5 nm OMP (blue), 2.4 nm $[RuCp^*mes]_2$ (purple) and 2.4 nm $[RuCp^*mes]_2$ + 5 nm OMP (yellow). Work functions and HOMO onsets are indicated by numbers. Spectra are vertically offset for clarity.

The corresponding UPS spectra are shown in Figure 3. Upon deposition of ca. monolayer of 1,2,3,4,7,8-hexafluoro-11,11,12,12-tetracyanonaphtho-2,6-quinodimethane (F_6TCNNQ) the work function of Ti_3C_2-T_x increased up to 5.69 eV (red/purple curve). No binding energy shifts in the Ti_3C_2-T_x core levels were observed (see Ti2p spectra in Figure S1, Supporting

Information), indicating the absence of band bending, as expected for a metal. Upon deposition of ca. monolayer of (pentamethylcyclopentadienyl)(1,3,5-trimethylbenzene)ruthenium dimer ([RuCp*Mes]$_2$, which is cleaved into two monomers with very low ionization energy after deposition, as described in detail elsewhere)[38,41] the work function of Ti_3C_2-T_x was reduced to 2.44 eV (blue/purple curve), again without any induced band bending observed (Figure S1, Supporting Information). Virtually any intermediate work function value between the two extremes can be achieved by employing appropriate sub-monolayer coverage of the respective donor/acceptor molecules (Figure S2, Supporting Information). This method allows covering a very broad work function range of 3.25 eV. Different orientations of the molecules due to, *e.g.*, different deposition parameters, could quantitatively change the work function change, but not the qualitative trend.[42] To put this into perspective, we summarized Ti_3C_2-T_x work function values found in literature from experiment and theory in Figure 4.[12,13,22,43–54] This comparison illustrates that: (i) a wide spread can be observed for as-prepared samples, ranging from 3.77 eV to 5.28 eV, with an average of 4.6±0.4 eV. These values brace the range of 4.64 eV to 5.19 eV that we observed for as-prepared samples after annealing at ≈350 °C in this work. (ii) Only a few attempts have been made to date to tune the work function of Ti_3C_2-T_x, with moderate success (maximum range 0.9 eV). The minimal and maximal work function values of 2.44 eV and 5.69 eV achieved in the present work span a much wider range and approach the predicted theoretical extreme work function values of 1.86 eV and 6.14 eV for Ti_3C_2-T_x with pure -OH or -O terminations, respectively,[19] as indicated by the dashed lines in Figure 4.

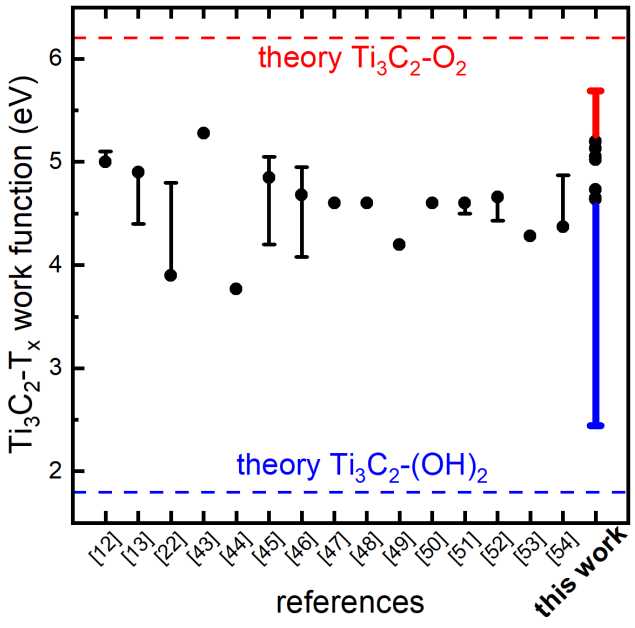

Figure 4: Ti_3C_2-T_x work function values found in the literature compared to those obtained in this work. The error bars indicate an intended change of the work function. The dashed lines indicate values predicted by density functional theory calculations for pure surface terminations.[19]

Energy level alignment tuning

To show how the work function tuning demonstrated above can be utilized to control the energy level alignment between Ti_3C_2-T_x and a subsequently deposited organic semiconductor, we chose a newly synthesized perylene derivative, namely 1,1,2,2,7,7,8,8-octamethyl-1,2,7,8-tetrahydrodicyclopenta[*cd,lm*]perylene (OMP), because this method allows at the same time the determination of ionization energy and electron affinity of this molecule, as demonstrated later. The synthesis details, nuclear magnetic resonance and mass spectra can be found in the Supporting Information, section S3. Its structure is shown in Figure 1, and the corresponding UPS data in Figure 3. When 5 nm of OMP are deposited onto pristine Ti_3C_2-T_x the work function is reduced from initially 5.19 eV (purple curve) to 4.61 eV and two distinct peaks appear in the valence band spectrum (green/purple curves). The lowest binding energy peak with a maximum at ≈1 eV is assigned to stem from the HOMO level of OMP and the neighboring peak with a maximum at 2.85 eV is assigned to the HOMO-1. With the HOMO onset at 0.61 eV (corresponding to the hole injection barrier at this interface) and the sample work function of 4.61 eV the ionization energy of OMP on Ti_3C_2-T_x can be determined to 5.22 eV. This is very close to the work function of the pristine Ti_3C_2-T_x and will therefore already lead to minute electron transfer from OMP to the Ti_3C_2-T_x substrate, accompanied by the formation of an interface dipole that lowers the sample work function compared to the pristine MXene surface. This phenomenon is known as *intrinsic* Fermi level pinning at the HOMO level.[55] When the work function of Ti_3C_2-T_x is increased to 5.69 eV with the ca. monolayer F_6TCNNQ, the results after OMP deposition are qualitatively the same (green/red/purple curves). However, the hole injection barrier, defined as the energy difference between the Fermi level at 0 eV binding energy and the HOMO onset, is in this case reduced to 0.32 eV. When OMP is deposited on the $[RuCp^*Mes]_2$-modified Ti_3C_2-T_x, with a work function of 2.44 eV, a slight increase in work function to 2.66 eV is observed (green/blue/purple curves). This indicates electron transfer from the modified Ti_3C_2-T_x substrate to the LUMO level of OMP, respectively referred to as Fermi level pinning at the LUMO level. From this observation we can infer that the electron affinity of OMP is around 2.3 eV, assuming similar HOMO/LUMO level shapes and therefore comparable hole/electron injection barriers.[56] This yields an electronic band gap of OMP of about 2.9 eV. The measured HOMO onset in this case is 2.67 eV, a significant change of +2.35 eV compared to OMP on an F_6TCNNQ interlayer. The energy level diagrams derived for both interlayers from our UPS data are shown in Figure 5, which evidently demonstrates how the energy level alignment between Ti_3C_2-T_x and OMP is changed from a minimal hole injection barrier in the case of an F_6TCNNQ interlayer to a minimal electron injection barrier in the case of an $[RuCp^*Mes]_2$ interlayer. The universal applicability of this interlayer method, for different substrates and different organic molecules and polymers, has been demonstrated before.[39,57,58] Based on the attained work function range, minimal injection barriers to organic semiconductors with ionization energies (electron affinities) as high (low) as about 6.0 eV (2.1 eV) should be achievable, thus tremendously expanding the range of possible organic materials to be used in devices with Ti_3C_2-T_x as an electrode.

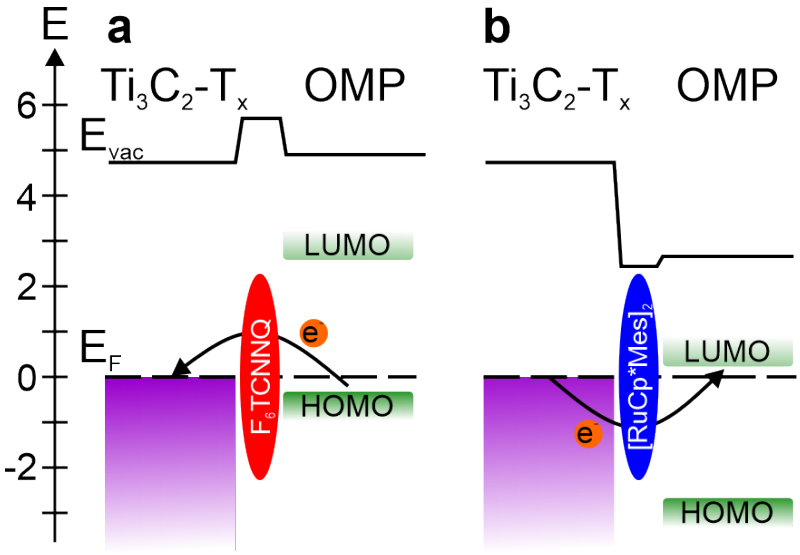

Figure 5: Energy level diagram derived from the measurements shown in Figure 2. With the help of a thin interlayer of acceptor/donor molecules the energy level alignment between Ti_3C_2-T_x and OMP can be tuned from a) minimal hole injection barrier using F_6TCNNQ to b) minimal electron injection barrier using $[RuCp^*Mes]_2$. All energy values are in eV.

Work function of predominantly oxygen-terminated Ti_3C_2-O_x

From theoretical calculations, it is predicted that surface termination has a huge impact on the work function of Ti_3C_2-T_x.[19,24] Surfaces terminated purely with oxygen are predicted to have a high work function of up to 6.2 eV, while purely hydroxyl terminated surfaces are predicted to have a very low work function as low as 1.8 eV. However, none of these surfaces with pure terminations was experimentally realized until 2020 when Persson *et al.* demonstrated a way to potentially produce purely oxygen-terminated Ti_3C_2-O_2 by an initial high-temperature annealing to remove fluorine terminations and a subsequent mild annealing at 100 °C in 2 mbar of oxygen.[59] We repeated this sample treatment to test if indeed very high work function values can be achieved in this way. The corresponding X-ray photoelectron spectroscopy (XPS) and UPS spectra are shown in Figure 6 for a low temperature (≈350 °C) annealing (black curves), a high temperature (≈750 °C) annealing to remove fluorine terminations (red curves), and a subsequent oxygen exposure at 2 mbar and ≈100 °C to saturate the surface with oxygen termination (blue curves). As observed by Persson *et al.* and also in our previous study,[22,59,60] the fluorine content decreases by about 80 % after high-temperature annealing. This can be seen both in the survey spectra (Figure S4a, Supporting Information) as well as in the narrow scans of the fluorine F1s region in Figure 6a. They exhibit only one peak, corresponding to the fluorine surface termination of Ti_3C_2-T_x. A complete removal could not be achieved, in agreement with previous reports, which moreover confirmed the structural stability at these elevated temperature by thermogravimetric analysis and transmission electron microscopy.[22,60] The O1s spectra in Figure 6b show significant changes in line shape, ascribed to a rearrangement of the oxygen atoms from the initially occupied bridge and hexagonal close-packed (HCP) sites to the face-centered cubic (FCC) site.[22] The Ti2p spectra in Figure 6c were fitted with a model suggested by Natu *et al.*, which comprises four peaks corresponding to different numbers of oxygen and fluorine atoms

bound to titanium.[61] All fit parameters are listed in the Supporting Information, section S5. However, this model does not consider different adsorption sites. A valence band peak at around 9 eV, ascribed to the fluorine, is strongly reduced and peaks related to oxygen termination groups at around 3 eV and 6 eV become more pronounced, as can be seen in Figure S4c in the Supporting Information.[22] The initial work function of 4.64 eV is reduced to 4.45 eV, in agreement with previous observations and calculations that predict the work function of bare Ti_3C_2 to be slightly lower than fluorine terminated Ti_3C_2-F_2.[19,22] After oxygen exposure the spectral shapes of the O1s and Ti2p spectra change again. Person *et al.* showed, by electron diffraction and residual gas analysis, that the structure of Ti_3C_2-T_x is stable up to 400 °C during 2 mbar O_2 exposure, so structural changes can be ruled out as cause for the observed changes in the XPS spectra.[59] Fitting of the O1s spectrum suggests a re-occupation of the bridge and hexagonal-close packed sites, as the FCC sites are already occupied by the initially present oxygen. The Ti2p spectrum shows an increase in intensity between 456 eV and 459 eV. This is the region that Natu *et al.* attribute to Ti-(OOF), Ti-(OFF) and Ti-(FFF) bonds. However, since the reoccupation with fluorine can be ruled out due to the absence of fluorine during oxygen exposure, the increase in intensity in this region must have a different origin. This emphasizes that the unambiguous fitting of the Ti2p core level of Ti_3C_2-T_x remains challenging. Part of the intensity increase around 459 eV can likely be ascribed to the beginning of TiO_2 formation, as also observed by Persson *et al.*, only for higher temperatures during oxygen exposure.[59] The origin of the intensity increase at lower binding energies (456-458 eV) remains unclear and requires complementary measurements to be unambiguously identified. The work function increases again, but only back to 4.65 eV, which is far from the theoretically predicted value of more than 6 eV. The question arises: Why is there such a large discrepancy between experiment and theory? The small amount of residual fluorine termination is very likely not the case, as Vito *et al.* explicitly calculated the work function for mixed terminations and obtained a value of close to 6 eV for our surface termination composition (6% fluorine, 94% oxygen).[24] Taking the average of the work function values of the purely terminated surfaces predicted by Khazaei *et al.* yields the same result.[19] The beginning formation of TiO_2 is likely not the reason as well, as this contribution is too small (<7%) to significantly contribute to the average work function measured by UPS for multicomponent surfaces.[62] Typical work functions for TiO_2 are around 4 eV,[63] which would result in an average work function of Φ_{avg}=0.07·4 eV +0.93·6 eV=5.86 eV, much higher than observed here. One potential explanation for the difference between experiment and calculations could be different absorption sites present in experiment and assumed in theory. While density functional theory (DFT) calculations assume one single termination site,[19,24] we find that oxygen adsorbs on multiple sites. We demonstrated before that the use of real surface termination compositions in DFT calculations leads to work function values much closer to experiment compared to averaged work function values of purely terminated surfaces, due to the electronic interplay between the different termination types and sites.[22] We therefore suggest that theoretical calculations should consider the actual surface composition and adsorption sites to get more realistic work function values. Furthermore, a recent theoretical study by Björk and Rosen suggested a way of fully removing termination groups of MXenes by annealing in H_2 atmosphere and the possibilities of termination with other terminal groups, demonstrating the potential for further experimental work beyond the scope of this study.[64] Lastly, the stability of these emerging structures as the Ti_3C_2-T_x and the

organic molecules are exposed to ambient conditions remains to be investigated, but is beyond the scope of this work.

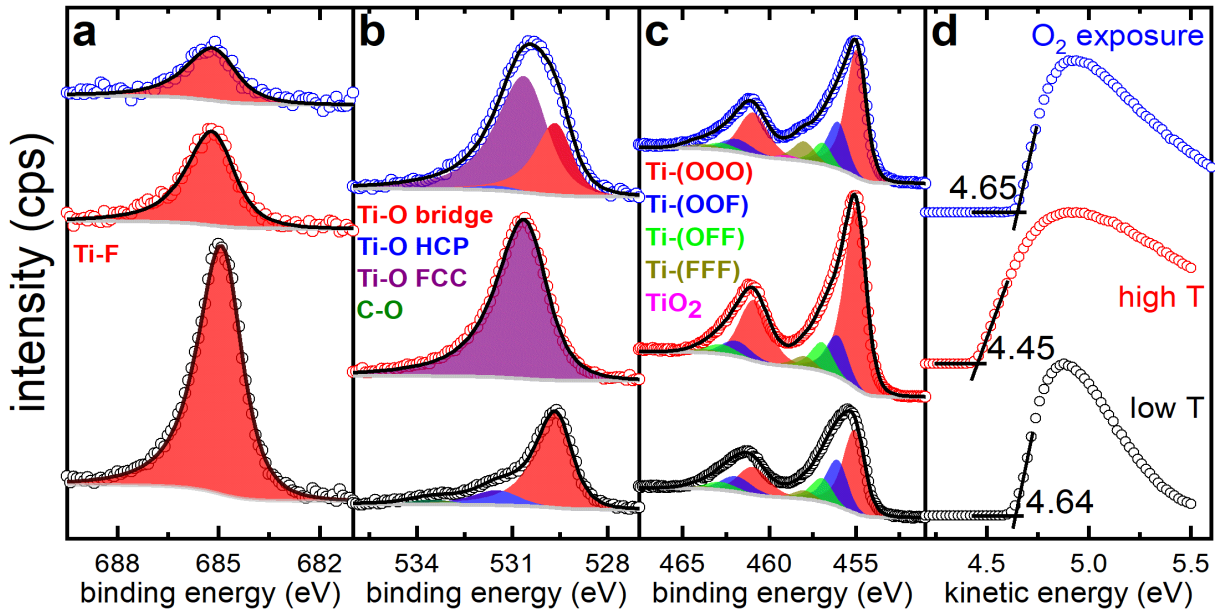

Figure 6: XPS and UPS results of Ti_3C_2-T_x annealed at 350 °C (black), 750°C (red) and after subsequent oxygen exposure at 2 mbar and 100 °C (blue). a) F1s core level spectra, b) O1s core level spectra, c) Ti2p core level spectra and d) secondary electron cut-off spectra. Spectra are vertically offset for clarity.

Conclusion

We first investigated the work function change of Ti_3C_2-T_x MXene upon deposition of (metal-)organic semiconductor molecules. Using the wide bandgap organic semiconductor CBP we found that only a small surface electron push-back effect is observed for Ti_3C_2-T_x, in line with the fact that its work function is strongly determined by the dipoles formed by the surface termination groups, which have a rather rigid electron density. Using the electron donor/acceptor molecules ($[RuCp^*Mes]_2$ and F_6TCNNQ we were able to tune the work function of Ti_3C_2-T_x within the remarkable range of 2.44-5.69 eV. Applying these molecules as interlayers to the subsequently deposited organic semiconductor OMP we were able to demonstrate achieving both minimal hole and minimal electron injection barriers. We predict that this should be achievable for organic semiconductors with ionization energies (electron affinities) as high (low) as about 6.0 eV (2.1 eV), which is highly attractive for numerous device applications where Ohmic contacts to organic semiconductors are needed. Furthermore, we showed that predominantly oxygen-terminated Ti_3C_2-O_x does not exhibit an extraordinarily high work function, in contrast to theoretical predictions. Overall, our findings will help to improve charge injection/extraction barriers in devices where Ti_3C_2-T_x is used as an electrode, and we encourage the exploration of alternative routes for work function tuning of Ti_3C_2-T_x (and other MXenes), beyond surface termination modifications only.

Methods

Sample preparation

MXene and MAX phases were synthesized according to our previous work.[65] Free-standing MXene films were prepared by vacuum-assisted filtration(Celgard®, 3501) 2 ml of the aqueous colloidal solution (1 mg mL^{-1}). The samples were dried under reduced pressure (10^{-3} mbar) at 110 °C for 12 h and afterwards only exposed to inert atmospheres (N_2, Ar).

With a short air exposure (<5 min) the MXene samples were introduced into a preparation chamber (base pressure 10^{-9} mbar) and initially annealed at ≈350 °C for half an hour to remove surface adsorbates. To remove fluorine, the samples were annealed at ≈750 °C for one hour. Oxygen exposure took place in a load lock (base pressure 10^{-8} mbar) at an oxygen partial pressure of 2 mbar for one hour, while the sample was illuminated with a halogen lamp to heat it up to ≈100 °C.

4,4′-bis(*N*-carbazolyl)-1,1′-biphenyl (CBP) was purchased from Sigma-Aldrich and 1,3,4,5,7,8-hexafluoro-11,11,12,12-tetracyanonaphtho-2,6-quinodimethane (F_6TCNNQ) was purchased from Novaled. (pentamethylcyclopentadienyl)(1,3,5-trimethylbenzene)ruthenium dimer ($[RuCp^*Mes]_2$) were synthesized as described elsewhere,[66] and 1,1,2,2,7,7,8,8-octamethyl-1,2,7,8-tetrahydrodicyclopenta[*cd,lm*]perylene (OMP) was synthesized as described in detail in the Supporting Information, section S3. All molecules were evaporated in the preparation chamber from resistively heated quartz crucibles. The nominal deposition rates were determined by a quartz crystal microbalance, assuming a density of 1.3 g/cm³, and were about 0.3-1 Å/min for CBP and the donor/acceptor molecules and about 1 nm/min for the OMP molecules.

Photoelectron spectroscopy

The photoelectron spectroscopy measurements were conducted at the ENERGIZE endstation at Bessy II. The base pressure in the analysis chamber was $2 \cdot 10^{-10}$ mbar. A DA30L analyzer from ScientaOmicron was used to detect the kinetic energy of the electrons, with a pass energy of 50 eV for X-ray photoelectron spectroscopy (XPS) measurements, a pass energy of 5 eV for the ultraviolet photoelectron spectroscopy (UPS) measurements of the valence band and a pass energy of 2 eV for the secondary electron cut-off (SECO) measurements. An achromatic DAR400 X-ray source from ScientaOmicron with an aluminum anode ($h\nu$=1486.6 eV) was used for excitation during XPS measurements and the He I excitation of an achromatic HIS13 He discharge lamp from ScientaOmicron was used during UPS measurements. This yields resolutions of 0.9 eV for XPS and 0.07 eV for UPS, respectively. A bias of -10V was applied to the sample during SECO measurements. The binding energy scale was calibrated by setting the center of the Fermi-edge of the Ti_3C_2-T_x samples to 0 eV binding energy. XPS core levels were fitted using CasaXPS,[67] applying an iterative Shirley-background. All peak fitting parameters are listed in the Supporting Information section S5.

Acknowledgements

Peer Bärmann and Tristan Petit acknowledge funding from the European Research Council (ERC) under the European Union's Horizon 2020 research and innovation programme (grant agreement No 947852). Elena Longhi, Stephen Barlow and Seth Marder acknowledge funding from the National Science Foundation through DMR-807797/2216857. Rahul Meena and Yves Geerts acknowledge funding from the European Union's Horizon 2020 research and innovation program under the Marie Sklodowska-Curie grant agreement No 811284 (UHMob). Yury Gogotsi's work on MXenes was supported by the National Science Foundation through DMR-2041050. The authors are grateful to Dr. Tyler Mathis for synthesis of MXene samples.

References

(1) Michałowski, P. P.; Anayee, M.; Mathis, T. S.; Kozdra, S.; Wójcik, A.; Hantanasirisakul, K.; Jóźwik, I.; Piątkowska, A.; Możdżonek, M.; Malinowska, A.; Diduszko, R.; Wierzbicka, E.; Gogotsi, Y. Oxycarbide MXenes and MAX Phases Identification Using Monoatomic Layer-by-Layer Analysis with Ultralow-Energy Secondary-Ion Mass Spectrometry. *Nat. Nanotechnol.* **2022**, 1–6.

(2) Bärmann, P.; Winter, M.; Gonzalez-Julian, J.; Placke, T. Solvent Co-Intercalation-Induced Activation and Capacity Fade Mechanism of Few-/Multi-Layered MXenes in Lithium Ion Batteries. *Small* **2021**, *17* (47), 2104130.

(3) Huang, L.; Li, T.; Liu, Q.; Gu, J. Fluorine-Free Ti3C2Tx as Anode Materials for Li-Ion Batteries. *Electrochem. commun.* **2019**, *104*, 106472.

(4) Xie, Y.; Naguib, M.; Mochalin, V. N.; Barsoum, M. W.; Gogotsi, Y.; Yu, X.; Nam, K. W.; Yang, X. Q.; Kolesnikov, A. I.; Kent, P. R. C. Role of Surface Structure on Li-Ion Energy Storage Capacity of Two-Dimensional Transition-Metal Carbides. *J. Am. Chem. Soc.* **2014**, *136* (17), 6385–6394.

(5) Pang, J.; Mendes, R. G.; Bachmatiuk, A.; Zhao, L.; Ta, H. Q.; Gemming, T.; Liu, H.; Liu, Z.; Rummeli, M. H. Applications of 2D MXenes in Energy Conversion and Storage Systems. *Chem. Soc. Rev.* **2019**, *48* (1), 72–133.

(6) Naguib, M.; Kurtoglu, M.; Presser, V.; Lu, J.; Niu, J.; Heon, M.; Hultman, L.; Gogotsi, Y.; Barsoum, M. W. Two-Dimensional Nanocrystals Produced by Exfoliation of Ti 3AlC 2. *Adv. Mater.* **2011**, *23* (37), 4248–4253.

(7) Anasori, B.; Lukatskaya, M. R.; Gogotsi, Y. 2D Metal Carbides and Nitrides (MXenes) for Energy Storage. *Nat. Rev. Mater.* **2017**, *2* (2), 1–17.

(8) Lipatov, A.; Alhabeb, M.; Lu, H.; Zhao, S.; Loes, M. J.; Vorobeva, N. S.; Dall'Agnese, Y.; Gao, Y.; Gruverman, A.; Gogotsi, Y.; Sinitskii, A. Electrical and Elastic Properties of Individual Single-Layer Nb4C3Tx MXene Flakes. *Adv. Electron. Mater.* **2020**, *6* (4), 1901382.

(9) Kamysbayev, V.; Filatov, A. S.; Hu, H.; Rui, X.; Lagunas, F.; Wang, D.; Klie, R. F.; Talapin, D. V. Covalent Surface Modifications and Superconductivity of Two-Dimensional Metal Carbide MXenes. *Science (80-.).* **2020**, *369* (6506), 979–983.

(10) Abdolhosseinzadeh, S.; Jiang, X.; Zhang, H.; Qiu, J.; Zhang, C. Perspectives on Solution Processing of Two-Dimensional MXenes. *Mater. Today* **2021**, *48*, 214–240.

(11) Shayesteh Zeraati, A.; Mirkhani, S. A.; Sun, P.; Naguib, M.; Braun, P. V.; Sundararaj, U. Improved Synthesis of Ti3C2T: XMXenes Resulting in Exceptional Electrical Conductivity, High Synthesis Yield, and Enhanced Capacitance. *Nanoscale* **2021**, *13* (6), 3572–3580.

(12) Ahn, S.; Han, T. H.; Maleski, K.; Song, J.; Kim, Y. H.; Park, M. H.; Zhou, H.; Yoo, S.; Gogotsi, Y.; Lee, T. W. A 2D Titanium Carbide MXene Flexible Electrode for High-Efficiency Light-Emitting Diodes. *Adv. Mater.* **2020**, *32* (23), 2000919.

(13) Lyu, B.; Kim, M.; Jing, H.; Kang, J.; Qian, C.; Lee, S.; Cho, J. H. Large-Area MXene Electrode Array for Flexible Electronics. *ACS Nano* **2019**, *13* (10), 11392–11400.

(14) Hantanasirisakul, K.; Zhao, M. Q.; Urbankowski, P.; Halim, J.; Anasori, B.; Kota, S.; Ren, C. E.; Barsoum, M. W.; Gogotsi, Y. Fabrication of Ti3C2Tx MXene Transparent Thin Films with Tunable Optoelectronic Properties. *Adv. Electron. Mater.* **2016**, *2* (6), 1600050.

(15) Mathis, T. S.; Maleski, K.; Goad, A.; Sarycheva, A.; Anayee, M.; Foucher, A. C.; Hantanasirisakul, K.; Shuck, C. E.; Stach, E. A.; Gogotsi, Y. Modified MAX Phase Synthesis for Environmentally Stable and Highly Conductive Ti3C2 MXene. *ACS Nano* **2021**, *15* (4), 6420–6429.

(16) Ling, Z.; Ren, C. E.; Zhao, M. Q.; Yang, J.; Giammarco, J. M.; Qiu, J.; Barsoum, M. W.; Gogotsi, Y. Flexible and Conductive MXene Films and Nanocomposites with High Capacitance. *Proc. Natl. Acad. Sci. U. S. A.* **2014**, *111* (47), 16676–16681.

(17) Arole, K.; Blivin, J. W.; Saha, S.; Holta, D. E.; Zhao, X.; Sarmah, A.; Cao, H.; Radovic, M.; Lutkenhaus, J. L.; Green, M. J. Water-Dispersible Ti3C2Tz MXene Nanosheets by Molten Salt Etching. *iScience* **2021**, *24* (12), 103403.

(18) Maleski, K.; Mochalin, V. N.; Gogotsi, Y. Dispersions of Two-Dimensional Titanium Carbide MXene in Organic Solvents. *Chem. Mater.* **2017**, *29* (4), 1632–1640.

(19) Khazaei, M.; Arai, M.; Sasaki, T.; Ranjbar, A.; Liang, Y.; Yunoki, S. OH-Terminated Two-Dimensional Transition Metal Carbides and Nitrides as Ultralow Work Function Materials. *Phys. Rev. B - Condens. Matter Mater. Phys.* **2015**, *92* (7), 75411.

(20) Liu, Y.; Guo, J.; Zhu, E.; Liao, L.; Lee, S. J.; Ding, M.; Shakir, I.; Gambin, V.; Huang, Y.; Duan, X. Approaching the Schottky-Mott Limit in van Der Waals Metal-Semiconductor Junctions. *Nature* **2018**, *557* (7707), 696–700.

(21) Park, S.; Schultz, T.; Shin, D.; Mutz, N.; Aljarb, A.; Kang, H. S.; Lee, C. H.; Li, L. J.; Xu, X.; Tung, V.; List-Kratochvil, E. J. W.; Blumstengel, S.; Amsalem, P.; Koch, N. The Schottky-Mott Rule Expanded for Two-Dimensional Semiconductors: Influence of Substrate Dielectric Screening. *ACS Nano* **2021**, *15* (9), 14794–14803.

(22) Schultz, T.; Frey, N. C.; Hantanasirisakul, K.; Park, S.; May, S. J.; Shenoy, V. B.; Gogotsi, Y.; Koch, N. Surface Termination Dependent Work Function and Electronic Properties of Ti3C2Tx MXene. *Chem. Mater.* **2019**, *31* (17), 6590–6597.

(23) Zhou, H.; Han, S. J.; Lee, H. D.; Zhang, D.; Anayee, M.; Jo, S. H.; Gogotsi, Y.; Lee, T. W.

Overcoming the Limitations of MXene Electrodes for Solution-Processed Optoelectronic Devices. *Adv. Mater.* **2022**, *34* (41), 2206377.

(24) Di Vito, A.; Pecchia, A.; Auf der Maur, M.; Di Carlo, A. Nonlinear Work Function Tuning of Lead-Halide Perovskites by MXenes with Mixed Terminations. *Adv. Funct. Mater.* **2020**, *30* (47), 1909028.

(25) Vázquez, H.; Dappe, Y. J.; Ortega, J.; Flores, F. Energy Level Alignment at Metal/Organic Semiconductor Interfaces: "Pillow" Effect, Induced Density of Interface States, and Charge Neutrality Level. *J. Chem. Phys.* **2007**, *126* (14), 144703.

(26) Sättele, M. S.; Windischbacher, A.; Greulich, K.; Egger, L.; Haags, A.; Kirschner, H.; Ovsyannikov, R.; Giangrisostomi, E.; Gottwald, A.; Richter, M.; Soubatch, S.; Tautz, F. S.; Ramsey, M. G.; Puschnig, P.; Koller, G.; Bettinger, H. F.; Chassé, T.; Peisert, H. Hexacene on Cu(110) and Ag(110): Influence of the Substrate on Molecular Orientation and Interfacial Charge Transfer. *J. Phys. Chem. C* **2022**, *126* (10), 5036–5045.

(27) Wagner, J.; Gruber, M.; Hinderhofer, A.; Wilke, A.; Bröker, B.; Frisch, J.; Amsalem, P.; Vollmer, A.; Opitz, A.; Koch, N.; Schreiber, F.; Brütting, W. High Fill Factor and Open Circuit Voltage in Organic Photovoltaic Cells with Diindenoperylene as Donor Material. *Adv. Funct. Mater.* **2010**, *20* (24), 4295–4303.

(28) Schultz, T.; Lungwitz, D.; Longhi, E.; Barlow, S.; Marder, S. R.; Koch, N. The Interlayer Method: A Universal Tool for Energy Level Alignment Tuning at Inorganic/Organic Semiconductor Heterojunctions. *Adv. Funct. Mater.* **2021**, *31* (10), 2010174.

(29) Lin, H.; Wang, X.; Yu, L.; Chen, Y.; Shi, J. Two-Dimensional Ultrathin MXene Ceramic Nanosheets for Photothermal Conversion. *Nano Lett.* **2017**, *17* (1), 384–391.

(30) Lv, K.; Yang, Q.; Yan, X.; Liang, L.; Liu, F.; Wang, M.; Yao, H.; Wei, D.; Ma, D.; Xie, K. Photosensitive Ti3C2 for Dyes Degradation. *Results Mater.* **2022**, *13*, 100247.

(31) Thibau, E. S.; Llanos, A.; Lu, Z. H. A Simple Rule for Determining the Band Offset at CH3NH3PbI3/Organic Semiconductor Heterojunctions. *Appl. Phys. Lett.* **2016**, *108* (2), 021602.

(32) Chin, B. D.; Suh, M. C.; Kim, M. H.; Lee, S. T.; Kim, H. D.; Chung, H. K. Carrier Trapping and Efficient Recombination of Electrophosphorescent Device with Stepwise Doping Profile. *Appl. Phys. Lett.* **2005**, *86* (13), 1–3.

(33) Niederhausen, J.; Amsalem, P.; Frisch, J.; Wilke, A.; Vollmer, A.; Rieger, R.; Müllen, K.; Rabe, J. P.; Koch, N. Tuning Hole-Injection Barriers at Organic/Metal Interfaces Exploiting the Orientation of a Molecular Acceptor Interlayer. *Phys. Rev. B - Condens. Matter Mater. Phys.* **2011**, *84* (16), 165302.

(34) Koch, N.; Kahn, A.; Ghijsen, J.; Pireaux, J. J.; Schwartz, J.; Johnson, R. L.; Elschner, A. Conjugated Organic Molecules on Metal versus Polymer Electrodes: Demonstration of a Key Energy Level Alignment Mechanism. *Appl. Phys. Lett.* **2003**, *82* (1), 70–72.

(35) Koch, N.; Duhm, S.; Rabe, J. P.; Vollmer, A.; Johnson, R. L. Optimized Hole Injection with Strong Electron Acceptors at Organic-Metal Interfaces. *Phys. Rev. Lett.* **2005**, *95* (23), 237601.

(36) Romaner, L.; Heimel, G.; Brédas, J. L.; Gerlach, A.; Schreiber, F.; Johnson, R. L.; Zegenhagen, J.; Duhm, S.; Koch, N.; Zojer, E. Impact of Bidirectional Charge Transfer and Molecular Distortions on the Electronic Structure of a Metal-Organic Interface. *Phys. Rev. Lett.* **2007**, *99* (25), 256801.

(37) Schultz, T.; Schlesinger, R.; Niederhausen, J.; Henneberger, F.; Sadofev, S.; Blumstengel, S.; Vollmer, A.; Bussolotti, F.; Yang, J. P.; Kera, S.; Parvez, K.; Ueno, N.; Müllen, K.; Koch, N. Tuning the Work Function of GaN with Organic Molecular Acceptors. *Phys. Rev. B* **2016**, *93* (12), 125309.

(38) Schlesinger, R.; Bianchi, F.; Blumstengel, S.; Christodoulou, C.; Ovsyannikov, R.; Kobin, B.; Moudgil, K.; Barlow, S.; Hecht, S.; Marder, S. R.; Henneberger, F.; Koch, N. Efficient Light Emission from Inorganic and Organic Semiconductor Hybrid Structures by Energy-Level Tuning. *Nat. Commun.* **2015**, *6* (1), 1–7.

(39) Schlesinger, R.; Xu, Y.; Hofmann, O. T.; Winkler, S.; Frisch, J.; Niederhausen, J.; Vollmer, A.; Blumstengel, S.; Henneberger, F.; Rinke, P.; Scheffler, M.; Koch, N. Controlling the Work Function of ZnO and the Energy-Level Alignment at the Interface to Organic Semiconductors with a Molecular Electron Acceptor. *Phys. Rev. B - Condens. Matter Mater. Phys.* **2013**, *87* (15), 155311.

(40) Schultz, T.; Niederhausen, J.; Schlesinger, R.; Sadofev, S.; Koch, N. Impact of Surface States and Bulk Doping Level on Hybrid Inorganic/Organic Semiconductor Interface Energy Levels. *J. Appl. Phys.* **2018**, *123* (24), 245501.

(41) Guo, S.; Mohapatra, S. K.; Romanov, A.; Timofeeva, T. V.; Hardcastle, K. I.; Yesudas, K.; Risko, C.; Brédas, J. L.; Marder, S. R.; Barlow, S. N-Doping of Organic Electronic Materials Using Air-Stable Organometallics: A Mechanistic Study of Reduction by Dimeric Sandwich Compounds. *Chem. - A Eur. J.* **2012**, *18* (46), 14760–14772.

(42) Wang, H.; Levchenko, S. V.; Schultz, T.; Koch, N.; Scheffler, M.; Rossi, M. Modulation of the Work Function by the Atomic Structure of Strong Organic Electron Acceptors on H-Si(111). *Adv. Electron. Mater.* **2019**, 1800891.

(43) Aydin, E.; El-Demellawi, J. K.; Yarali, E.; Aljamaan, F.; Sansoni, S.; Rehman, A.; Harrison, G.; Kang, J.; El Labban, A.; De Bastiani, M.; Razzaq, A.; Van Kerschaver, E.; Allen, T. G.; Mohammed, O. F.; Anthopoulos, T.; Alshareef, H. N.; De Wolf, S. Scaled Deposition of Ti3C2Tx MXene on Complex Surfaces: Application Assessment as Rear Electrodes for Silicon Heterojunction Solar Cells. *ACS Nano* **2022**, *16* (2), 2419–2428.

(44) Xu, X.; Guo, T.; Hota, M. K.; Kim, H.; Zheng, D.; Liu, C.; Hedhili, M. N.; Alsaadi, R. S.; Zhang, X.; Alshareef, H. N. High-Yield Ti3C2Tx MXene–MoS2 Integrated Circuits. *Adv. Mater.* **2021**, 2107370.

(45) Yang, C.; Qin, S.; Zuo, Y.; Shi, Y.; Bie, T.; Shao, M.; Yu, Y. Waveguide Schottky Photodetector with Tunable Barrier Based on Ti3C2Tx/p-Si van Der Waals Heterojunction. *Nanophotonics* **2021**, *10* (16), 4133–4139.

(46) Prabaswara, A.; Kim, H.; Min, J. W.; Subedi, R. C.; Anjum, D. H.; Davaasuren, B.; Moore, K.; Conroy, M.; Mitra, S.; Roqan, I. S.; Ng, T. K.; Alshareef, H. N.; Ooi, B. S. Titanium Carbide MXene Nucleation Layer for Epitaxial Growth of High-Quality GaN Nanowires on Amorphous Substrates. *ACS Nano* **2020**, *14* (2), 2202–2211.

(47) El-Demellawi, J. K.; Mansour, A. E.; El-Zohry, A. M.; Hedhili, M. N.; Yin, J.; Emwas, A. H. M.; Maity, P.; Xu, X.; Bakr, O. M.; Mohammed, O. F.; Alshareef, H. N. Tuning the Work Function of Ti3C2Tx MXene by Molecular Doping without Changing Its Surface Functional Groups. *ACS Mater. Lett.* **2022**, *10*, 2480–2490.

(48) Mariano, M.; Mashtalir, O.; Antonio, F. Q.; Ryu, W. H.; Deng, B.; Xia, F.; Gogotsi, Y.; Taylor, A. D. Solution-Processed Titanium Carbide MXene Films Examined as Highly Transparent Conductors. *Nanoscale* **2016**, *8* (36), 16371–16378.

(49) Chen, J.; Yang, B.; Lim, Y. D.; Duan, W.; Zhao, Y.; Tay, B. K.; Yan, X. Ti 3 C 2 (MXene) Based Field Electron Emitters. *Nanotechnology* **2020**, *31* (28), 285701.

(50) Hou, C.; Huang, C.; Yu, H.; Shi, S. Surface-Engineered Ti 3 C 2 T x with Tunable Work Functions for Highly Efficient Polymer Solar Cells. *Small* **2022**, *18* (21), 2201046.

(51) Yu, Z.; Feng, W.; Lu, W.; Li, B.; Yao, H.; Zeng, K.; Ouyang, J. MXenes with Tunable Work Functions and Their Application as Electron- and Hole-Transport Materials in Non-Fullerene Organic Solar Cells. *J. Mater. Chem. A* **2019**, *7* (18), 11160–11169.

(52) Wang, Z.; Kim, H.; Alshareef, H. N. Oxide Thin-Film Electronics Using All-MXene Electrical Contacts. *Adv. Mater.* **2018**, *30* (15), 1706656.

(53) Choi, J.; Kim, Y. J.; Cho, S. Y.; Park, K.; Kang, H.; Kim, S. J.; Jung, H. T. In Situ Formation of Multiple Schottky Barriers in a Ti3C2 MXene Film and Its Application in Highly Sensitive Gas Sensors. *Adv. Funct. Mater.* **2020**, *30* (40), 2003998.

(54) Huang, K.; Li, C.; Zhang, X.; Wang, L.; Wang, W.; Meng, X. Self-Assembly Synthesis of Phosphorus-Doped Tubular g-C3N4/Ti3C2 MXene Schottky Junction for Boosting Photocatalytic Hydrogen Evolution. *Green Energy Environ.* **2021**.

(55) Koch, N. Opportunities for Energy Level Tuning at Inorganic/Organic Semiconductor Interfaces. *Appl. Phys. Lett.* **2021**, *119* (26), 260501.

(56) Oehzelt, M.; Koch, N.; Heimel, G. Organic Semiconductor Density of States Controls the Energy Level Alignment at Electrode Interfaces. *Nat. Commun.* **2014**, *5* (1), 1–8.

(57) Schultz, T.; Schlesinger, R.; Niederhausen, J.; Henneberger, F.; Sadofev, S.; Blumstengel, S.; Vollmer, A.; Bussolotti, F.; Yang, J. P.; Kera, S.; Parvez, K.; Ueno, N.; Müllen, K.; Koch, N. Tuning the Work Function of GaN with Organic Molecular Acceptors. *Phys. Rev. B* **2016**, *93* (12).

(58) Schlesinger, R.; Bianchi, F.; Blumstengel, S.; Christodoulou, C.; Ovsyannikov, R.; Kobin, B.; Moudgil, K.; Barlow, S.; Hecht, S.; Marder, S. R.; Henneberger, F.; Koch, N. Efficient Light Emission from Inorganic and Organic Semiconductor Hybrid Structures by Energy-Level Tuning. *Nat. Commun.* **2015**, *6* (1), 6754.

(59) Persson, I.; Halim, J.; Hansen, T. W.; Wagner, J. B.; Darakchieva, V.; Palisaitis, J.; Rosen, J.; Persson, P. O. Å. How Much Oxygen Can a MXene Surface Take Before It Breaks? *Adv. Funct. Mater.* **2020**, *30* (47), 1909005.

(60) Persson, I.; Näslund, L. Å.; Halim, J.; Barsoum, M. W.; Darakchieva, V.; Palisaitis, J.; Rosen, J.; Persson, P. O. Å. On the Organization and Thermal Behavior of Functional Groups on Ti3C2 MXene Surfaces in Vacuum. *2D Mater.* **2018**, *5* (1), 015002.

(61) Natu, V.; Benchakar, M.; Canaff, C.; Habrioux, A.; Célérier, S.; Barsoum, M. W. A

Critical Analysis of the X-Ray Photoelectron Spectra of Ti3C2Tz MXenes. *Matter* **2021**, *4* (4), 1224–1251.

(62) Schultz, T.; Lenz, T.; Kotadiya, N.; Heimel, G.; Glasser, G.; Berger, R.; Blom, P. W. M.; Amsalem, P.; de Leeuw, D. M.; Koch, N. Reliable Work Function Determination of Multicomponent Surfaces and Interfaces: The Role of Electrostatic Potentials in Ultraviolet Photoelectron Spectroscopy. *Adv. Mater. Interfaces* **2017**, *4* (19).

(63) Zhu, L.; Lu, Q.; Lv, L.; Wang, Y.; Hu, Y.; Deng, Z.; Lou, Z.; Hou, Y.; Teng, F. Ligand-Free Rutile and Anatase TiO2 Nanocrystals as Electron Extraction Layers for High Performance Inverted Polymer Solar Cells. *RSC Adv.* **2017**, *7* (33), 20084–20092.

(64) Björk, J.; Rosen, J. Functionalizing MXenes by Tailoring Surface Terminations in Different Chemical Environments. *Chem. Mater.* **2021**, *33* (23), 9108–9118.

(65) Mathis, T. S.; Maleski, K.; Goad, A.; Sarycheva, A.; Anayee, M.; Foucher, A. C.; Hantanasirisakul, K.; Shuck, C. E.; Stach, E. A.; Gogotsi, Y. Modified MAX Phase Synthesis for Environmentally Stable and Highly Conductive Ti3C2 MXene. *ACS Nano* **2021**, *15* (4), 6420–6429.

(66) Un, H. I.; Gregory, S. A.; Mohapatra, S. K.; Xiong, M.; Longhi, E.; Lu, Y.; Rigin, S.; Jhulki, S.; Yang, C. Y.; Timofeeva, T. V.; Wang, J. Y.; Yee, S. K.; Barlow, S.; Marder, S. R.; Pei, J. Understanding the Effects of Molecular Dopant on N-Type Organic Thermoelectric Properties. *Adv. Energy Mater.* **2019**, *9* (24), 1900817.

(67) Fairley, N.; Fernandez, V.; Richard-Plouet, M.; Guillot-Deudon, C.; Walton, J.; Smith, E.; Flahaut, D.; Greiner, M.; Biesinger, M.; Tougaard, S.; Morgan, D.; Baltrusaitis, J. Systematic and Collaborative Approach to Problem Solving Using X-Ray Photoelectron Spectroscopy. *Appl. Surf. Sci. Adv.* **2021**, *5*, 100112.